Short title: Microdomain coordination between neighbors in plants

Authors:

Andreas Kolbeck[1,#], Peter Marhavý[1,#,¶], Damien De Bellis[1,2], Lothar Kalmbach[1,†] and Niko Geldner[1,§,‡]

Title: CASP microdomain formation requires cross cell wall stabilization of domains between neighbors and non-cell autonomous action of LOTR1 cell wall protein

Author affiliations

1 Department of Plant Molecular Biology, University of Lausanne, Lausanne, Switzerland

2 Electron Microscopy Facility, University of Lausanne, Lausanne, Switzerland

Author list footnotes

# These authors contributed equally

§ Corresponding author. Tel: +41 21 692 4192;
E-mail: niko.geldner@unil.ch

‡ Lead Contact

¶ Present address: Umeå Plant Science Centre (UPSC), Department of Forest Genetics and Plant Physiology, Swedish University of Agricultural Sciences (SLU), Umeå, Sweden

† Present address: Sainsbury Laboratory, University of Cambridge, Bateman Street, Cambridge CB2 1LR, UK

Summary

Efficient uptake of nutrients in both animal and plant cells requires tissue-spanning diffusion barriers separating inner tissues from the outer lumen/soil. However, we poorly understand how these contiguous three-dimensional superstructures are formed in plants. Here, we show that correct establishment of the plant Casparian Strip (CS) network requires neighbor communication. We show that positioning of Casparian Strip membrane domains (CSDs) is tightly coordinated between neighbors in wild-type and that restriction of domain formation involves the putative extracellular protease LOTR1. Impaired domain restriction in *lotr1* is associated with disrupted CSDs and establishment of fully functional CSD at ectopic positions, forming "half strips". LOTR1 is expressed in stele and needs to be expressed there. Endodermal expression, by contrast, cannot complement, while cortex expression causes a dominant-negative phenotype. Our findings establish *LOTR1* as a crucial player in CSD positioning acting in a non-cell-autonomous pathway to restrict and coordinate CS positioning.

Keywords

Endodermis, Casparian Strips, extracellular diffusion barriers, membrane domains, coordination, cell ablation

Introduction

Plants mine the surrounding soil for water and dissolved minerals to sustain their growth and to complete their life cycle. Likened to inverted guts, roots evolved crucial epithelial functions — selective uptake and diffusion barriers — in order to generate and sustain body homeostasis in variable and harsh environments. The required separation of outside lumen and inside tissues is achieved in gut epithelial cells through the formation of tight junctions. These specialized membrane domains form ring-like domains between the apical (gut lumen) and basal (blood stream) sides. Close adhesion of both adjacent plasma membranes is achieved by tight interaction of occludins, claudins, and cadherins, organized into tight and adherens junctions, forming impermeable and mechanically-resistant barriers. In plants, a functionally similar diffusion block is achieved by Casparian strips (CS), highly localized impregnations of the cell wall, the plant's extracellular matrix, in root endodermal cells.

Similar to tight/adherence junctions, a specialized membrane domain (Casparian Strip membrane Domain, CSD) forms a precise ring in transversal and anticlinal membranes of elongated endodermal cells. This domain acts as a molecular fence that separating the endodermal plasma membranes into peripheral (outer) and central (inner) domains, highlighted by the polar distribution of nutrient transporters (Julien Alassimone, Naseer, and Geldner 2010; Bao et al. 2019; Ma et al. 2007; Takano et al. 2010). CASPARIAN STRIP DOMAIN PROTEINs (CASPs) are specifically targeted to this domain and form a stable matrix for the subsequent lignification machinery (Roppolo et al. 2011; Lee et al. 2013; Hosmani et al. 2013; Kalmbach et al. 2017; Barbosa, Rojas-Murcia, and Geldner 2019). Lignification of the primary cell wall of CSs extends through the entire apoplast including cross-linkage to the middle lamella. This is illustrated in cell wall digestions leaving only the resistant lignified tissues of CSs and xylem visible as a fishnet-like matrix (Enstone, Peterson, and Ma 2002).

The CS and tight/adherens junctions must form a contiguous network in order to fulfill their role as functional diffusion barriers. However, we still

81 poorly understand how such a supracellular structure is coordinated within
82 a cell layer such as the endodermis. Although we are ignorant of the
83 mechanism, the precisely opposing localization of CSDs evidences that
84 endodermal cells coordinate the positioning of their membrane domains
85 across the cell wall space. In epithelial cells, adherens junctions are first
86 initiated by cell-to-cell contact mediated by nectins and cadherins and kept
87 in place by firm attachment to the actin cytoskeleton (Rajasekaran et al.
88 1996; Itoh and Bissell 2003). In plant cells, their cell wall matrices separate
89 neighboring cell by more than 100 nm, which prevents such a direct
90 interaction of membrane bound proteins. Still, a more complex positioning
91 mechanism that requires local signals from directly adjacent neighbors
92 would ensure coordination of CSDs with the correct neighbor.

93 Many components necessary for correct CS formation have been identified
94 in recent years, but few show impacts on CS positioning *per se*. Mutation of
95 components in the recently discovered barrier surveillance mechanism
96 causes interrupted, but correctly localized CSDs (Pfister et al. 2014; Doblas
97 et al. 2017; Nakayama et al. 2017; J Alassimone et al. 2016). Loss of the
98 endodermal differentiation transcription factor MYB36 abolishes the
99 formation of the entire CSD while disruption of CS cell wall localised ESB1
100 causes unstable, but still correctly localised domains (Kamiya et al. 2015;
101 Liberman et al. 2015; Hosmani et al. 2013). The recently published *lotr2*
102 mutant revealed the importance of a member of the exocyst complex,
103 *EXO70A1*, in mediating targeted secretion of CASP proteins to the pre-
104 established CSD (Kalmbach et al. 2017). However, the fragmented domains
105 visible in this mutant are non-functional and unstable. Thus, based on
106 current data, it is unclear whether formation of functional CSDs at ectopic
107 positions is even possible.

108 Here, we report that the recently discovered *lotr1* mutant forms fully
109 functional CSDs outside the endodermal-endodermal cell interface in. We
110 establish that neighbouring endodermal cells are absolutely required to
111 form stable and continuous CSDs and we highlight close coordination of CSD
112 microdomains during the early stages of domain formation. In addition, we

113 demonstrate that *LOTR1* is crucial for restriction of the CSD and that it acts
114 independently of any known pathway for CSD formation. We show that this
115 new type of putative cell wall protease is expressed in the stele and acts in
116 a novel non-cell-autonomous signalling pathway that controls CSD stability
117 in the endodermis. We thus demonstrate that CS positioning is both directly
118 and indirectly coordinated between endodermal cells to ensure correct
119 positioning of this crucial membrane domain and open up new pathways for
120 investigation.

121

122 **Results**

123 *Ectopic CASP deposits in lotr1 are fully functional CSDs*

124 During their initial characterization of the *lotr1* mutant, Li et al. 2017
125 reported a novel 'patchy' phenotype, where large patches of the Casparian
126 strip membrane domain marker CASP1::CASP1-GFP occurred outside of the
127 regular median CS position. Further analysis revealed an apoplastic delay
128 phenotype attributed to large gaps that could be observed in the CS upon
129 lignin stain. We performed a more detailed analysis of the domain marker
130 CASP1::CASP1-GFP in this mutant background to search for disruptions in
131 the CSD that could explain these gaps in lignification. Confirming the earlier
132 findings (Li et al. 2017), we found large patches of CASP1-GFP occurring in
133 endodermal membranes that were never observed in wildtype plants (Fig.
134 1B). Whereas previously reported to occur only facing pericycle cells, we
135 found similar patches to also occur towards the outer cortex (Fig. 1B, Fig S1),
136 although quantification revealed a clear preference for the endodermal-
137 pericycle interface. In addition to these patches, we found disruptions of the
138 central CSD which occurred primarily at cell corners with nearby ectopic
139 CASP deposits (Fig. 1B), coherent with the reported gaps in CS lignin. The
140 overall correctly positioned and largely continuous central CSD in *lotr1*
141 suggests that the core-localization mechanism for the CSD is still functional.
142 We speculate that the change in cell shape and cell walls at junctions might
143 favor patch formation in *lotr1*. If patch formation starts simultaneously with
144 initial focalization of CASPs into micro-domains (known as the string-of-

145 pearls stage), nearby ectopic CASP deposits might inhibit the growth of the
146 central domain leading to the observed large discontinuities. In order to
147 better understand the nature and origin of these patches, we followed CASP
148 deposition throughout endodermal differentiation. In both wildtype and
149 *lotr1*, CASP1-GFP aggregated into aligned micro-domains in the cell's median
150 (Fig. S1C). During this initial focalization step, we observed occurrence of
151 ectopic CASP islands in *lotr1*, indicating a role of LOTR1 during this early step
152 of defining the CS location. Ectopic CASP deposits grew over time and were
153 able to fuse into larger patches, similarly to the central micro-domains
154 combining into a continuous ring. We did not observe degradation of these
155 patches nor formation of new patches once the central domain was fused,
156 confirming that these patches are stable once formed and their
157 establishment is restricted to the short developmental window in which the
158 cells determine their CS location. Consequently, LOTR1 likely acts in this
159 early phase as an inhibitor of ectopic domain formation. We then
160 investigated whether these patches represent fully functional domains, i.e.
161 whether they are able to guide lignification enzymes to these sites.
162 Deposition of lignin can be easily identified in electron microscopy, where
163 CSs are visible as a clearly defined, homogenous stretch of cell wall spanning
164 the entire apoplastic space (Roppolo et al. 2011; Fujita et al. 2020) (Fig. S1D).
165 Ultra-structure analysis of *lotr1* revealed similar cell wall modifications in
166 pericycle-facing endodermal membranes (Fig. 1D).To our surprise, and in
167 contrast to regular CSs, this ectopic lignin patch was restricted to the
168 endodermal part of the cell wall, stopping precisely at the middle lamella,
169 effectively creating half of a Casparian Strip. Such a strict spatial
170 confinement of lignification on a nanometer scale is quite surprising since
171 monolignols and ROS, both essential for lignin polymerization, are thought
172 to be mobile in cell walls and lignin polymerization itself not to be under
173 direct enzymatic control. To our knowledge, such a strictly restricted
174 lignification encompassing only half of a thin primary has not been observed
175 previously. Our finding therefore suggests a very local and directed lignin
176 polymerization in the CS, where each endodermal cell is responsible for
177 lignifying their part of the cell wall to build a functional CS barrier. A

178 functional CSD is also characterized by a tight attachment of the underlying
179 membrane, which is revealed in EM by the mild plasmolysis of the plasma
180 membrane introduced through sample preparation, which is absent at the
181 CSD. Perfectly matching the cell autonomous nature of the ectopic patches,
182 tight attachment of the endodermal membrane, but not the pericycle
183 membrane was observed.

184 In order to further support our hypothesis that *lotr1* ectopic patches are fully
185 functional domains, we compared consecutive electron micrograph sections
186 with and without potassium permanganate ($KMnO_4$) staining to check for
187 lignification. Depositing electron dense material by reaction with lignin
188 sidechains, $KMnO_4$ highlights lignin presence as darkening of cell walls in CSs
189 and protoxylem vessels (Stein, Klomparens, and Hammerschmidt 1992;
190 Yamashita et al. 2016). Ectopic patches in *lotr1* displayed KMnO4 staining on
191 the endodermal side of the half-strips, while the opposite pericycle cell walls
192 were unstained (Fig. 1E). This correlated with CS-typical cell wall appearance
193 (more homogenous, less electron-dense, slightly thickened) observed in
194 unstained consecutive cuts, confirming lignin presence at these ectopic
195 domains. Notably, several samples displayed CS-type cell wall morphology
196 with accompanying membrane attachment and lignification throughout the
197 entire endodermal cell corner, stretching from the median endodermal-cell
198 interface all the way to the endodermal-pericycle cell walls (Fig. S1E).
199 Although ectopic lignification is a hallmark of many Casparian Strip mutants,
200 this was not described for *lotr1.* Furthermore, enhanced lignification itself
201 does not result in firm membrane attachment outside the regular CS.
202 Consequently, this points to a drastically enlarged CSD indicative of an
203 impaired ability to restrict CSD growth in *lotr1,* agreeing with a presumed
204 role of LOTR1 as inhibitor of domain formation.

205 The regular CSD recruits a multitude of enzymes required for restricted
206 monolignol polymerization to form the CS. The tightly restricted lignin
207 accumulation at ectopic *lotr1* patches suggested similar recruitment of these
208 enzymes. Indeed, when we co-expressed the CSD marker CASP1-GFP
209 together with typical members of this lignin machinery in *lotr1* to confirm

210 their recruitment to ectopic CSDs. Endodermis specific PEROXIDASE 64
211 (PRX64) and LACCASE 3 (LAC3) displayed a clear co-labelling in both central
212 and ectopic domains while NADPH oxidase RbohF, the main generator of
213 ROS for monolignol polymerization, was also found to be present, although
214 it did not specifically accumulate there (Fig. 1F). Finally, we analyzed the
215 localization of dirigent-domain protein ESB1 in *lotr1*. Although it was
216 previously reported to be absent from ectopic deposits (Li et al. 2017). We
217 found ESB1 to accumulate at the sites of ectopic CASP1-deposition when
218 expressed as ESB1-mCherry under its native promoter together with CASP1-
219 GFP. Dirigent-domain proteins are thought to be a key component in
220 restricting and directing lignin polymerization in the cell wall (Hosmani et al.
221 2013), which was evident in CSs as well as patches in *lotr1* in our ultra-
222 structure analysis. Our results of ESB1 localization therefore agree with
223 PER64 and LAC3 labelling, as well as the tight restriction of lignin at these
224 patches, proving these ectopic formations to be fully functional, but
225 ectopically formed CSDs.

226 *Focalization of CASPs is coordinated between cells*

227 The fact that an ectopic CSD patch towards a non-endodermal neighbor can
228 only induce formation of a half-strip suggested that two neighboring
229 endodermal cells absolutely need to align their respective CSDs in order to
230 lignify the entire CS cell wall space. To ensure this, a mechanism would need
231 to be in place that promotes formation of a CSD at places where a
232 neighboring cell is forming one and/or inhibits CSD formation in the absence
233 of a neighboring CSD. We therefore investigated the initial focalization of
234 CASP proteins at high resolution. When properly aligned along the z-axis, we
235 were able to identify two distinct membrane signals present between two
236 neighboring endodermal cells (Fig. 2A,C). Strikingly, at the string-of-pearls
237 stage, CASP1-GFP intensity along the length of both signals already showed
238 a strong positive correlation (R^2 = 0.535, p = 1.612 e-9) (Fig. 2B), indicating
239 coordination of CSD formation across the cell wall already at this stage. To
240 validate our assumption that these paired signals represent the signals of
241 neighboring cell membrane domains, we checked the position of CS cell wall

242 protein ESB1 and cell wall tracer Propidium Iodide (Fig. 2B+C). In contrast to
243 CASP1-GFP, ESB1-mCherry localized in a single line in between the observed
244 CASP-labelled membranes in both early and late CSDs (Fig. 2C). To further
245 confirm that these GFP signals truly represented separate membranes, we
246 decided to employ cell-specific laser ablation to destroy one of the cells,
247 arguing that this should remove only one half of the paired signal. Indeed,
248 upon ablation, GFP signal was specifically lost in the ablated cell whereas the
249 adjacent signal of the intact neighboring cell was unchanged (Fig. 2D,E).
250 Together, our data demonstrate the observed double signals to be adjacent
251 CSDs of neighboring endodermal cells, whose initial formation is tightly
252 coordinated between cells. We then investigated whether currently known
253 mutants such as *sgn1*, *sgn3* and *esb1* would display defects in CASP
254 microdomain coordination (Fig. S2). However, all these mutants showed
255 wildtype like coordination between adjacent CSDs. Interestingly, *lotr1* also
256 showed well-coordinated deposition of micro-domains at the Casparian strip
257 position. Therefore, while LOTR1 appears to be necessary to restrict,
258 unpaired, ectopic domain establishment, its loss-of function does not seem
259 to affect the process of coordination at the correct central position where
260 the future CS between neighboring cells is forming. This is corroborated by
261 the lack of CS half-strips at the regular median position between endodermal
262 cells in *lotr1*.

263 *Endodermal cells require a neighboring cell to stabilize CASPs*

264 The close correlation of CASP micro-domains in neighboring endodermal
265 membranes could be explained by an unknown feedback control mechanism
266 that stabilizes microdomains upon presence of neighboring domains and de-
267 stabilizes them in their absence. Such a mechanism would immediately
268 guide CSD formation towards endodermis-endodermis surfaces. In order to
269 test this model, we ablated individual endodermal cells in the elongation
270 zone, prior to their transition to differentiation. This enabled us to compare
271 CSD establishment with and without a functional neighbor in the same cell.
272 Initially, we observed CASP deposition in a string-of-pearls-typical pattern in
273 membranes facing living and dead cells alike (Fig. 3A,D). However, only

274 membranes facing intact neighbors were able to form a continuous strip,
275 whereas domains towards ablated cells did not progress past the string-of-
276 pearls stage. When we ablated all adjacent cells, the single intact cell was
277 still able to express and focalize CASPs but was unable to establish any
278 continuous domains (Fig. 3C). We also noticed a strong difference in signal
279 intensity between membranes facing living and dead cells, where GFP signal
280 increased rapidly in CSDs towards intact neighbors, but not ablated cells (Fig.
281 3B). This discrepancy is likely a result of an inability to recruit additional CASP
282 proteins to the initially formed micro-domains. This suggested a control
283 point during CSD establishment where a neighboring signal is required to
284 progress from the string-of-pearls stage and commit to formation of a CS.
285 We had to exclude that isolating endodermal cells from their neighbors by
286 ablation might cause stresses that influence overall endodermal
287 differentiation and not just a destabilization of CASP recruitment to the
288 membrane. We therefore used a CASP1 transcriptional reporter, driving a
289 nuclear fluorescent protein. Upon ablation of all surrounding endodermal
290 cells a similar CASP promoter activity compared to non-affected cells was
291 observed, indicating that progress of differentiation *per se* was not halted in
292 the isolated cell (Fig. S3A). To rule out possible general effects on secretion
293 or localization of plasma membrane proteins, we then ablated cells in
294 double marker lines expressing CASP1-GFP and the generic SYP122-
295 3xmCherry plasma membrane marker, both under the control of the CASP1
296 promoter. Again, this clearly established that isolated cells still express from
297 the CASP1 promoter. Moreover, they accumulate SYP122 on all cell sides, in
298 contrast to CASP1, which accumulates only at plasma membrane domains
299 facing a living neighbor (Fig. 3D).

300 We then thought to confirm our findings by means that do not involve
301 destruction of neighboring cells. To do so we generated inducible
302 complementation lines for MYB36, a key transcription factor of endodermal
303 differentiation (Liberman et al. 2015; Kamiya et al. 2015). *MYB36* loss-of-
304 function mutants are unable to activate expression of key CSD proteins, e.g.
305 CASPs, and consequently lack a CSD. Using very low level of inducer, we

306 generated sporadic MYB36 activation to enable some, but not all cells to
307 start differentiation and initiate CS formation. Expectedly, we observed a
308 sporadic, patchy expression pattern of CSD domain marker CASP1-GFP upon
309 induction, with some samples displaying expression in isolated, single cells,
310 while others showed cell groups with a near complete CSD network (Fig. 3E).
311 Confirming our ablation results, we found that isolated cells were able to
312 deposit CASP1-GFP in typical micro-domains but were incapable of forming
313 a stable and continuous CSD, similar to what was observed using cell
314 ablation (Fig. 3E). If two adjacent cells started to deposit CASPs, we observed
315 an increase in GFP signal only in the domain between these cells, followed
316 by fusion of the initial micro-domains into a continuous strip. The domains
317 not facing a CASP1 expressing neighbor did not progress beyond a string-of-
318 pearls stage and eventually lost the CASP1-GFP signal (Fig. 3F, S3B). We
319 conclude that wildtype plants appear to require signals from neighbors to
320 form stable microdomains and commit to a CS. *lotr1* is currently the only
321 known mutant that can form functional microdomains in the absence of
322 neighbors. We therefore asked whether *lotr1* might be able to fuse micro-
323 domains at the side facing the dead neighbor into continuous strips. Yet,
324 when we ablated cells in *lotr1,* we observed a similar disappearance of the
325 central CSD facing the ablated cell (Fig S3C). One explanation could be that
326 LOTR1 function is redundant for destabilization of unpaired domains in the
327 correct, central position, but is required at surfaces facing non-endodermal
328 neighbors. Indeed, we did observe formation of stable, *lotr1*-typical patches
329 on the side facing its dead neighbor, although they occurred in membranes
330 facing alive pericycle cells.

331 *LOTR1 defines a novel pathway controlling CASP domain positioning*

332 While no other knock-out mutant resembles *lotr1*, overstimulation of the
333 SCHENGEN (SGN) pathway by external application of CIF2 peptide, leads to
334 ectopic formation of CASP domains somehow resembling the phenotype of
335 *lotr1*. The CIF2 peptide is perceived by the Leucine-rich repeat receptor
336 kinase SGN3 (also called GSO1), a key receptor controlling a novel apoplastic
337 barrier surveillance pathway (Doblas et al. 2017; Nakayama et al. 2017). A

338 complete absence of SGN3 activity in knock-out mutants leads to an
339 incomplete fusion of otherwise correctly positioned CASP micro-domains. In
340 order to test, whether *lotr1* ectopic patches are due to an overactive SGN
341 pathway, we generated double knockouts of *lotr1* in combination with *sgn1*,
342 *sgn2* or *sgn3*. Single mutants *sgn1* and *sgn2* showed sporadic disruptions in
343 their central CSD while *sgn3* displayed more numerous holes in comparison,
344 agreeing with previously published data (J Alassimone et al. 2016; Doblas et
345 al. 2017) (Fig. 4A). Double mutants displayed *lotr1*-typical ectopic deposition
346 of CASP1-GFP, as well as discontinuities of the central domain. Although
347 discontinuities in the central CSDs were visible in *lotr1* itself, these occurred
348 mostly at cell junctions, while *sgn*-typical interruptions were present
349 throughout the length of the CSD. Both types of disruptions were found in
350 the respective double mutants. Moreover, no significant difference between
351 the double and single mutants was observed in blockage of apoplastic tracer
352 PI, a test for CS functionality (Fig 4C). This clear additivity of phenotypes
353 suggests that LOTR1 and SGN mutants are involved in separate pathways. It
354 certainly excludes a model whereby ectopic patch formation of *lotr1* is due
355 to an overactive SGN pathway. We also tested a possible connection to ESB1.
356 Again, *lotr1 esb1* double mutants displayed a mixture of parental
357 phenotypes with an *esb1*-typical string-of-pearl-stage central CSD and *lotr1*-
358 typical ectopic CASP deposits and showed no enhanced apoplastic barrier
359 phenotype, indicating that LOTR1 also acts independently of esb1 in CS
360 domain formation.

361 The model of SGN3-CIF1/2 integrity signaling predicts enhanced lignification
362 of endodermal cell corners and an early onset of suberization whenever the
363 diffusion barrier is broken in such a way that CIF peptides cannot be
364 restricted anymore. The previously described enhanced suberin phenotype
365 in *lotr1* is consistent with such a barrier-defect induced activation of the SGN
366 pathway, due to its large corner gaps in the CS domain. the previously
367 reported large gaps in lignification of CSs (Li et al., 2017), fit the
368 discontinuous CSDs in this mutant. Presence of $KMnO_4$-stained lignin
369 throughout the endodermal cell corners found in some samples during our

370 ultra-structural analysis (Fig. S1E) resembledSGN3-induced ectopic
371 lignification. To unambiguously demonstrate ectopic lignin deposition
372 outside the CASP-labelled domain, we employed a novel clearing protocol
373 that enables co-observation of fluorescent markers, e.g. CASP1-GFP, and
374 lignin specific stains, such as Basic Fuchsin (Ursache et al. 2018) (Fig. S4A).
375 Additional to the central CS, lignin accumulates at ectopic CASP1-deposits in
376 *lotr1*, further confirming these patches to be fully functional CSDs (FIG 4B).
377 Cell corner lignification not associated with CASP1 domains was observed at
378 sites of gaps in the CSDs within a cell, but not at places where the CSD was
379 continuous. This nicely supports the recently proposed model in which
380 SGN3-stimulation can induce local lignification with subcellular precision
381 (Fujita et al. 2020). Consistently, enhanced lignin deposition in cell corners
382 was not present in the *lotr1 sgn3* double mutant, confirming this ectopic
383 lignin to be caused by activation of the barrier surveillance mechanism.*lotr1*-
384 typical patches, by contrast, were still lignified in the double mutant,
385 supporting the concept of two separate pathways controlling lignin
386 deposition in the endodermis: A developmental lignification pathway
387 building up CS-type lignin and the SGN3-mediated ectopic lignin deposition
388 that compensates in case of barrier defects. Exogenous application of CIF2
389 peptide further demonstrated that the SGN3-pathway is functional in *lotr1*
390 (Fig. 4D). In the presence of CIF2, both genotypes formed ectopic lignin at
391 cell corners.

392 *LOTR1 is broadly expressed in the root*

393 Due to a lack of available expression data in public databases (*LOTR1* was
394 not included on the ATH1 microarrays), it was crucial to generate a reporter
395 line. We therefore placed a nuclear-localized tdTomato under the control of
396 a 3 kb LOTR1 promoter fragment. We observed strong promoter activity in
397 the root meristem in nearly all tissue layers and cells, including QC and
398 columella, with the highest expression found in the stele (FIG 4E). Very low
399 expression was found in the entire cortex cell linage, where promoter
400 activity was visible in the cortex/endodermal initial and its endodermis
401 daughter cell, but not in the cortex daughter. In older meristematic cells,

402 *LOTR1* expression further reduced in epidermis and endodermis, whereas
403 stele cells continued to show strong promoter activity. This pattern
404 continued past the elongation zone, where stele expression was still strong
405 with some residual signals found in epidermal and endodermal cells. Inside
406 the stele itself, *LOTR1* was specifically absent in xylem precursor and xylem-
407 adjacent procambium cells, whereas pericycle, phloem precursor and
408 phloem-adjacent procambium cells displayed strong expression (FIG 4E).
409 Recently published single-cell RNA sequencing results showed strong
410 expression of LOTR1 in clusters corresponding to phloem, stele, xylem, and
411 root cap cells, confirming our promoter activity analysis (Ryu et al. 2019;
412 Denyer et al. 2019). Despite this broad expression pattern, *lotr1* mutants
413 displayed only phenotypes related to endodermal differentiation, i.e.
414 ectopic CASP deposition and disrupted CSDs causing compensatory
415 lignification and suberin deposition, which themselves are likely responsible
416 for the previously observed delay in lateral root development and low-
417 calcium-sensitivity phenotype (Li et al. 2017). Consequently, if the
418 expression pattern points to a much broader function for LOTR1 outside of
419 endodermal differentiation, these additional functions are probably
420 redundantly fulfilled some of the many homologs of LOTR1 (Fig. 4F).

421 *LOTR1* codes for a putative cell wall protein with a predicted signal peptide,
422 a putative auto-inhibitory domain (Neprosin-AP), and a Neprosin domain,
423 recently identified as novel proline protease domain in an enzyme found in
424 the digestive fluids of pitcher plants (Rey et al. 2016; Schrader et al. 2017).
425 We found 42 other proteins in the Arabidopsis proteome with a domain
426 structure like LOTR1, i.e. having both Neprosin-AP and Neprosin domains,
427 although subsequent phylogenetic analysis showed considerable variation
428 among the family members. Average identity towards LOTR1 among this
429 "HOMOLOGS-OF-LOTR1" (HOLO) family was only 38 % (± 12) with the three
430 closest homologs standing out at ~ 70 % (Table S1). Phylogenetic clustering
431 identified 5 subgroups (A:E) with instances of gene-duplication events visible
432 especially in group C, where 8 homologs were found in consecutive loci on
433 chromosome 4, highlighting the variable nature of this family (Fig. 4F).

434 Nevertheless, putative orthologs of LOTR1 can be identified in both mono-
435 and eudicot species, indicating that, although some family members seem
436 to evolve rapidly, LOTR1 has a deep conservation of function, expected for a
437 regulator of CS formation.

438 While 34 of the putative homologs showed predicted signal peptides for
439 apoplastic localization, we also found 5 proteins in the family predicted to
440 have a single N-terminal transmembrane domain with their active domain
441 outside in the apoplast (Fig. 4F, Table S1). Thus, the HOLO family are
442 interesting candidates for proteolytically processing membrane or cell wall
443 proteins relevant for domain establishment. Single-cell RNAseq expression
444 profiles of *LOTR1's* four closest homologs partially overlapped in cell clusters
445 for QC/meristem (At1g23340, At1g70550, At5g56530), root cap (At1g10750,
446 At1g70550), phloem (At1g70550, At5g56530), and xylem (At1g10750,
447 At23340, At1g70550, At56530) (Ryu et al. 2019), explaining the lack of any
448 meristematic phenotypes in *lotr1*. However, while 8 separate mutants with
449 this unique patchy phenotype identified in the *LORD-OF-THE-RINGS* screen
450 all turned out to be alleles of *LOTR1*, none of its homologs were found,
451 indicating they likely have separate roles.

452 Mature and active Neprosin has been reported to consist only of its
453 functional domain (PF03080) (Rey et al. 2016), presumably undergoing
454 processing during or after secretion. However, only full-length protein was
455 found in functional, full-length complementation lines (Fig. S4C), suggesting
456 that LOTR1 might retain its putative auto-inhibitory Neprosin-AP domain.
457 Expression of artificially truncated versions of LOTR1 consisting of only its
458 Neprosin domain or only its putatively auto-inhibitory Neprosin-AP domain
459 resulted in extensive intracellular labelling and non-functional
460 complementation (Fig. S4D), supporting that LOTR1 does not undergo post-
461 processing.

462 As many of the Neprosin-containing proteins are still annotated as putative
463 carboxyterminal proteases, we investigated potential homologies towards
464 such enzymes. Database searches identified *E.coli* protein mepS, a cell wall
465 protease required for cell wall expansion, as a potential candidate. Although

466 displaying only 20 % identity to LOTR1's Neprosin domain, structural
467 comparison revealed that three crucial amino acids of mepS's catalytic
468 center, one cysteine and two histidines, are present in LOTR1, its three
469 closest homologs, and Neprosin (Fig. S5A,B). Expression of a full-length
470 LOTR1 version with putative active-site residues C255 and C260 mutated to
471 alanine showed apoplastic localization similar to unmutated LOTR1, but was
472 unable to complement the *lotr1* phenotype (Fig. S4D). This suggests an
473 important functional role for these amino acids in LOTR1 and supports a
474 protease function for this enzyme class in *Arabidopsis*.

475 *Tissue specific complementation indicates a non-cell autonomous action for*
476 *LOTR1.*

477 The strong expression pattern of LOTR1 suggests a function in the inner stele
478 tissues and a non-autonomous action of LOTR1 on endodermal
479 differentiation. With a potential protease function an action on the equally
480 stele-expressed CIF peptides was conceivable, but inconsistent with our
481 genetic analysis. In order to establish the site of LOTR1 action, we generated
482 LOTR1 fusion proteins and were able to complement the loss-of-function
483 phenotype with LOTR1 N-terminal (behind the signal peptide), but not C-
484 terminal fusion proteins, indicating that a free C-terminus is important for
485 its functionality (Fig. 5A). Interestingly, the *lotr1-8* allele, where a late STOP-
486 codon truncated the protein by just 16 aa leads to a knock-out phenotype,
487 further suggesting an important role of the c-terminal extremity. In
488 agreement with the promoter activity, fluorescence of the fusion construct
489 was mainly visible in the apoplastic space between stele cells, with outer
490 tissues showing very low levels of accumulation.

491 To determine if the very low expression observed in the endodermis is
492 nonetheless responsible for LOTR1 function, we generated lines driving
493 LOTR1 expression from stele-, endodermal-, or cortex-specific promoters in
494 the *lotr1* mutant background. We found continuous CSDs and lack of patches
495 only when expressed from the stele specific SHORTROOT (SHR) and CIF2
496 promoters, but not from endodermal SCR, CASP1, and ELTP, nor cortex
497 specific C1 promoters (Fig. 5C). Covering early, middle, and late endodermal

498 development, the lack of complementation by endodermal promoters
499 demonstrated that LOTR1 was not acting in the endodermis to fulfil its role
500 in CSD formation. Peculiarly, expression of the same construct under the
501 ubiquitous 35S CaMV promoter did also not complement the underlying
502 *lotr1* phenotype. Several scenarios could explain this finding: LOTR1 function
503 could require exclusive expression in the stele, although its native promoter
504 showed some weak outer tissue activity. Alternatively, over- and
505 misexpression of the construct might lead to the same patchy *lotr1*
506 phenotype, but through dominant interference. We therefore created an
507 inducible complementation construct, where the 3kb *LOTR1* promoter
508 fragment was fused to the estrogen-inducible artificial XVE transcription
509 factor, with a subsequent minimal 35S promoter driving expression of the
510 native gene (Zuo, Niu, and Chua 2000; Siligato et al. 2016). This allows
511 control of expression strength of the target genes. Upon induction of this
512 construct in the *lotr1* background, we observed a full complementation of
513 the phenotype even under strong induction conditions (Fig. 5B). Control
514 plants without inducer showed the typical phenotype. Thus, expression
515 strength was not causing the lack of complementation in the 35S lines,
516 leaving mis- expression in outer tissues as a probable cause for the observed
517 phenotype.

518 We therefore tested whether ubiquitous expression via 35S would lead to a
519 dominant-interference phenotype in wildtype. We outcrossed all generated
520 lines to wildtype CASP1-GFP plants to test for genetic dominance of the
521 transformed constructs. Previously complementing constructs
522 LOTR1::LOTR1, SHR::LOTR1, and CIF2::LOTR1 continued to display a wild-
523 type CSDs and no occurrence of *lotr1* typical patches in the F1 generation
524 (Fig. 5C). Wild-type phenotypes were also observed for the non-
525 complementing, endodermis-specific SCR and CASP1 driven lines.
526 Remarkably, not only expression driven by 35S, but also from cortex-specific
527 C1 and endodermal/cortex-expressing ELTP promoters caused ectopic
528 CASP1-GFP patches like those observed in uncomplemented *lotr1* in the F1
529 progeny. We confirmed this dominant phenotype in the following

530 segregating F2 generations, where all plants harboring ELTP, C1, or 35S
531 constructs showed patch formation. Only 7/37 (ELTP), 9/42 (C1), and 8/45
532 (35S) plants displayed wildtype like continuous CSDs and no patches in the
533 respective F2 populations. Since the dominant phenotype was not easily
534 distinguishable from the normal *lotr1* loss-of-function phenotype, our
535 observed ratios (18.9 %, 21.4 %, 17.7 %) matched the expected 3/16 (18.75
536 %) Mendelian segregation ratio for a wildtype phenotype. Apoplastic barrier
537 functionality tests in these lines confirmed our observations (Fig. 5D).

538

539 **Discussion**

540 Establishment of a functional apoplastic barrier relies on the correctly
541 localized deposition of lignin at the median position between endodermal
542 cells (Naseer et al. 2012; Geldner 2013). Although many components
543 involved in this process have been identified in the last decade, we still
544 poorly understand the mechanism by which these cells achieve the precise
545 formation of Casparian Strips in such a way that a single, thin, continuous
546 ring of lignin is formed in between endodermal cells. In our current work, we
547 provide new insights into this mechanism by demonstrating strict
548 coordination of CASP deposition in membranes of adjacent endodermal
549 cells. Independent of any known CS mutant, this coordination pathway
550 appears to allow a local initial pairing of forming CASP micro-domains, across
551 the cell wall of neighboring endodermal cells, which promotes their
552 stabilization and eventual fusion. This results in the necessity for having a
553 functional, differentiating endodermal cell neighbors in order to form a
554 continuous CS. Without a neighboring cell in the same developmental state,
555 wild-type endodermal cells abort CS development after the initial formation
556 of CASP microdomains, which eventually disappear. In our current
557 understanding, CASPs are initially secreted in a non-localized fashion
558 (Roppolo et al. 2011), yet rapidly form aligned CASP micro domains. This is
559 initiated by a specific exocyst complex, defined by subunit EXO70A1, whose
560 accumulation at the site of the future CS precedes CASP accumulation and is
561 necessary for their targeted secretion to this domain (Kalmbach et al. 2017).

562 Accordingly, EXO70A1 mutants display a high number of non-localized and
563 non-functional, unstable CASP microdomains. What mechanism could
564 account for the selective stabilization of CASPs in domains facing intact
565 neighbors of the same differentiation state, but not towards dead,
566 undifferentiated cells or cells of a different cellular identity? One explanation
567 would postulate the existence of a stabilizing short-range signal, produced
568 by CASPs domain that can only act *in trans*, not *in cis*. However, such an
569 exclusive *in trans* action is difficult to conceive with small, released
570 molecules able to diffuse across the cell wall space. It would be much easier
571 to conceive with filaments, reaching across the cell walls between domains,
572 but there is no evidence for the existence of such filament-like structures.
573 Alternatively, a cumulative threshold for a short-range, stabilizing signal
574 produced by the microdomains could be postulated, that could only be
575 reached when both cells produce it. However, such a model would require a
576 very finely tuned thresholding. Although a promising candidate for a factor
577 involved in this coordination process, our detailed analysis of the *lotr1*
578 mutant demonstrates that it does not affect the coordination of the properly
579 localized micro-domains between cells, nor does it allow for their formation
580 without neighbors. Nevertheless, absence of LOTR1 activity clearly allows
581 for formation of non-paired, stable, and fully functional microdomains,
582 oriented towards non-endodermal neighbors. Therefore, it is most likely
583 responsible for inhibiting sporadic micro-domain formation throughout the
584 endodermal membrane when CASPs are starting to focalize from their
585 ubiquitous distribution in the plasma membrane into aligned micro-
586 domains. The peculiar formation of Casparian half-strips in *lotr1*, further
587 indicates that lignin deposition into the CS cell wall is separately performed
588 by both contributing cells, which would make a tight coordination of
589 neighboring CASP domains all the more critical for achieving a fully sealed
590 cell wall space. Restricted mostly to the stele in mature regions of the root,
591 we provide evidence that this putative cell wall protease might act on a
592 target originating outside of its own expression profile. *lotr1* could only be
593 complemented using stele-specific promoters and neither endodermal,
594 cortex nor ubiquitous expression leads to complementation. Importantly we

595 discovered that wildtype plants displayed a dominant *lotr1*-like phenotype
596 with ectopic patches, disrupted CSDs, and a corresponding delay in PI block
597 when LOTR1 was mis-expressed in the cortex. How could ectopic expression
598 of a putative cell wall protease in the cortex interfere with the action of the
599 same protease in its wild-type expression domain in the stele? The most
600 parsimonious explanation we can conceive is that a LOTR1 substrate is
601 produced in the outer cortical tissues and has to diffuse into the stele for
602 activation by stele-expressed LOTR1 (Fig. 5E). Expression of LOTR1 in the
603 cortex would lead to a premature activation of its substrate in the cortex and
604 not allow it to reach the stele. It would thus deplete the endogenous LOTR1
605 of its substrate and cause the observed dominant loss-of-function
606 phenotype. In summary, this explanation draws a reverse-type SGN3/CIF
607 pathway model where a cortex-specific substrate passes across the
608 endodermal cell layer to be activated by a stele-specific enzyme complex,
609 destabilizing CASPs and preventing domain formation at ectopic positions.

610

611 **Acknowledgments**

612 We wish to thank the Central Imaging Facility (CIF) and the Electron
613 Microscopy Facility (EMF) of the University of Lausanne for their technical
614 expertise. We also thank Hiroko Uchida and Marie Barberon for their
615 graphical work. This work was supported by an ERC Consolidator Grant
616 (GA-N°: 616228—ENDOFUN) and two SNSF grants (CRSII3_136278 and
617 31003A_156261) to N.G., and a Federation of European Biochemical
618 Sciences Postdoctoral Long-Term Fellowship to P.M..

619 **Author contributions**

620 AK, PM, LK, and NG conceived and designed the project. AK, PM, and DDB
621 performed experiments and AK and PM performed image quantification. AK
622 and NG wrote the manuscript and all authors revised the manuscript.

623

624 **Declaration of Interests**

625 The authors declare that they have no conflict of interest.

626 **Figure legends**

627 **Fig. 1: Ectopic domain formation in *lotr1.***

628 A Schematic representation of endodermal maturation with stages of
629 Casparian Strip (CS) development (green). Elongated endodermal cells
630 focalize CASP1-GFP into aligned micro-domains which are subsequently
631 fused into a continuous ring around each endodermal cells.

632 B CASP1-GFP localization in wildtype and *lotr1* with focus on patch
633 localization. Images depict maximum intensity projections of z-stack
634 images. 3D reconstruction image depicts region indicated in *lotr1* overview
635 image, section view images are annotated by yellow (top) and blue
636 (bottom) arrows. Overview images scale bars: 20 µm; 3D reconstruction &
637 section views scale bars: 10 µm.

638 C 3D schematic for visualization of median endodermal cell section with
639 annotated cell faces.

640 D TEM section of *lotr1* obtained at 2 mm from root tip. Overview of section
641 with focus on regular CS and adjacent ectopic patch. Closeup indicated by
642 dashed black line in overview image; en = endodermis, pe = pericycle, co =
643 cortex, scale bars = 2 µm.

644 E Consecutive TEM sections at 2 mm from root tip, with and without
645 $KMnO_4$ staining, position indicated in (D). Dark deposits indicate electron-
646 dense MnO_2 precipitation caused by reaction with lignin. Note that in the
647 case of ectopic patches, the staining is restricted to the endodermal side of
648 the cell wall; en = endodermis, pe = pericycle, interspaced white line
649 depicts extend of CS-like cell wall morphology, scale bar = 1 µm.

650 F Localization of enzymes necessary for CS lignification in wildtype Col-0
651 and *lotr1*, pictures depict cells as seen in (C). Cellulosic cell walls are stained
652 with Calcofluor White and depicted in white in overlay images, scale bar =
653 10 µm.

654

655 **Fig. 2: CASP deposition is coordinated between neighboring endodermal**
656 **cells.**

657 A Double membrane phenotype visible with CASP1::CASP1-GFP during
658 string-of-pearls stage of CS development, scale bars depict 10 µm. Red and
659 grey arrows indicate separate membranes measured in (B).

660 B Comparison of GFP intensity between adjacent membranes indicated in
661 (A). Pixel intensity was measured along each membrane and relative GFP
662 intensity was adjusted to mean intensity of each membrane. Correlation of

663 original intensities (R-squared) was determined by fitting of a linear model
664 with indicated probability of fit (p-value).

665 C Localization of CSD marker CASP1-GFP in comparison to cell wall protein
666 ESB1-mCherry at early and mature CSs, scale bar depicts 5 µm.

667 D,E Double membrane phenotype of CASP1-GFP before and after ablation
668 of one adjacent endodermal cell in early (D) and late (E) CSs. Cell walls (red)
669 are stained with Propidium iodide (PI), yellow arrows indicate intensity
670 profiles measured in F-I; asterisks indicate ablated cell, scale bars = 5 µM.

671 F-I Quantification of CASP1-GFP and PI intensity before and after cell
672 ablation. Intensity was quantified in a 7-pixel wide line indicated in (D) and
673 (E).

674

675 **Fig. 3: Endodermal neighbors are required for proper CSD establishment**

676 A Endodermal cell ablation leads to instability of the CSD in membranes
677 facing dead cells. Endodermal cells were ablated 3-5 cells prior to onset of
678 CASP1-GFP (white) expression and followed over indicated time spans. First
679 image depicts overview after ablation with cells outlined with PI; # depicts
680 remaining live endodermal cell, dashed yellow line depicts cell outlines of
681 ablated cells, arrow indicates onset of CASP expression, dashed green and
682 red rectangles indicate quantification areas shown in (B), scale bar = 20
683 µm.

684 B Quantification of GFP fluorescence over time in membranes facing live
685 (green) and dead (red) adjacent endodermal cells. Intensity depicted in
686 relation to maximum total GFP intensity.

687 C Ablation of all adjacent endodermal cells prevents fusion of CSDs.
688 Endodermal neighbors were ablated at timepoint 0 and CASP1-GFP
689 expression (white) followed over time in remaining cell (#), PI (red)
690 highlighted cell outlines and confirmed destruction of cells; yellow arrow
691 indicates initial CASP microdomains, scale bar = 50 um.

692 D CASP instability in membranes facing ablated cells is independent from
693 CASP expression. Cells ablated 3-5 cells prior to onset of CASP expression,
694 cell outline depicted with dashed yellow line, arrow indicates stable CASP
695 formation, scale bar = 100 um.

696 E CASP fusion occurs only if both neighboring cells reach expression
697 threshold. Endodermal differentiation was induced via 0.5 µM β-estradiol
698 and CASP1-GFP expression followed over the next 12 h. Yellow arrows
699 indicate CASP deposits in the membrane, dashed green and red rectangles
700 indicate areas for quantification shown in (F).

701 F Quantification of GFP fluorescence over time in membranes reaching
702 local stability threshold (green) and those below the threshold (red).

703

704 **Fig. 4: LOTR1 restricts CSD establishment through independent pathway.**

705 A CASP1-GFP fluorescence of known CS mutants in wildtype and *lotr1*
706 background. Yellow arrows indicate parental CS mutant phenotype while
707 blue arrows highlight *lotr1* specific phenotypes; scale bar = 20 um.

708 B Enhanced lignification in *lotr1* is SCHENGEN-dependent. Ectopic lignin
709 (magenta) accumulates in *lotr1* at disruptions of the CASP1-GFP (green)
710 marked CSD. Lignification of the central domain and ectopic patches is
711 unaffected by disruption of *SGN3*, scale bar = 20 um.

712 C Apoplastic barrier phenotypes of *lotr1* double mutants. Formation of
713 apoplastic barrier was determined by penetrance of apoplastic tracer PI to
714 the stele; n = 10, significance determined by one-way ANOVA and separate
715 groups identified with Tukey-Kramer test.

716 D SCHENGEN-pathway is unaffected in *lotr1*. Wildtype and *lotr1* seedlings
717 were treated for 24 h with 100 µM synthetic CIF2 peptide and lignin
718 accumulation (magenta) outside the regular CSD domain (green) analysed.
719 Cell walls were stained with Calcofluor White, yellow arrows indicate
720 ectopic lignin accumulation, scale bar = 5 µm.

721 E LOTR1 expression indicates additional roles. Promoter activity highlighted
722 by tdTomato fluorescence in 5 day old seedlings; cells outlined by
723 Propidium iodide (white); mid-view regions depicted below highlighted by
724 continuous rectangles (a,b) and section views indicated by dash-dotted
725 lines (c,d), inlay shows colour profile of *LOTR1* expression intensity. a
726 Single-plane section through root meristem region, arrow indicates cortex-
727 daughter cell. b Single-plane section after cell elongation, arrows indicate
728 expression in endodermis (top arrow) and epidermis (bottom arrow). c
729 Maximum-intensity projection of section view of z-stack through meristem
730 region indicated in top picture. d Maximum-intensity projection of section
731 view of z-stack through mature region indicated in top picture; * denotes
732 endodermal cell lineage, scale bars: *top*: 100 um; *a*,*b*: 20 um; *c*,*d*: 50 um.

733 F Phylogenetic analysis of *HOMOLOGS-OF-LOTR1* (HOLO) family in
734 *Arabidopsis thaliana*. Homologs of LOTR1 in *A.thaliana* were identified and
735 grouped into five subfamilies by phylogenetic distance, LOTR1 (At5g50150)
736 highlighted in red, underlined genes have predicted N-terminal
737 transmembrane domains.

738 **Fig. 5: Stele-specific LOTR1 is restricts CSD establishment through a**
739 **cortex-expressed, mobile target.**

740 A Complementation of *lotr1* phenotype. N-terminal fusion construct
741 expressed under native *LOTR1* promoter complements ectopic CSD
742 phenotype. Scale bars: *left* 100 um, *section views* 20 um.

743 B Overexpression of *LOTR1* in wild-type and *lotr1* backgrounds does not
744 affect complementation. CASP1-GFP phenotype of seedlings grown for 5
745 days on control or 5 µM β-estradiol; scale bar: 20 um.

746 C Mis-expression of LOTR1 in cortical cells causes dominant loss-of-
747 function phenotypes. CASP1-GFP phenotypes of seedlings expressing
748 LOTR1-complementation construct used in (A) under indicated promoters.
749 Activity of used promoter indicated in schematics below; blue arrows
750 indicate *lotr1*-like phenotypes; EP = epidermis, CO = cortex, EN =
751 endodermis, ST = stele; scale bars = 20 um.

752 D Apoplastic barrier phenotypes of tissue specific complementation lines in
753 wildtype (white) and *lotr1* (grey) background. Cells after onset of
754 elongation counted until penetrance of PI was blocked. n = 10, significance
755 determined via one-way ANOVA and independent groups identified via
756 Tukey-Kramer post-hoc test.

757

758 **STAR Methods**

759 *Plant material and growth conditions*

760 All experiments were performed in the *Arabidopsis thaliana* Columbia-0
761 ecotype. T-DNA insertion lines obtained from NASC: *lotr1-10*
762 (SALK_051707) (Li et al. 2017), *sgn3-3* (SALK_043282) (Pfister et al. 2014),
763 *sgn1-2* (SALK_055095C) (J Alassimone et al. 2016), *sgn2-2* (SALK_009847)
764 (Doblas et al. 2017); *myb36-2* (GK- 543B11) (Kamiya et al. 2015), *esb1-1*
765 was kindly shared by Prof. David Salt's group (Hosmani et al. 2013), and the
766 *lotr1-1* allele was identified in the *LOTR*-screen (Li et al. 2017). Inducible
767 pUBQ10>>XVE::MYB36 were obtained from the TRANSPLANTA collection
768 (N2102512 and N2102513) and crossed to CASP1::CASP1-GFP. If not
769 otherwise stated, plants were grown as follows: Seeds were surface
770 sterilized and sown on half-strength Murashige-Skoog medium (Duchefa)
771 solidified with 0.8 % plant agar (Duchefa). After stratification for 2 days at 4
772 °C, seeds were germinated in growth chambers with long-day conditions
773 (16 h light/8 h dark) and temperature cycling between 22 °C/19 °C
774 (day/night). 5 days after germination, seedlings were directly analysed or
775 cleared and stained with ClearSee as described (Ursache et al. 2018). For
776 long-term imaging, agar blocks with seedlings were cut and transferred
777 into microscope chamber slides (Marhavý and Benková 2015; Marhavý et
778 al. 2016) and equal volume of double-concentrated β-estradiol added
779 before imaging.

780 *Plasmid construction*

781 A 3 kb promoter fragment of *LOTR1* was generated by 5'-
782 aacaggtctcgacctctttctatctgtttgtacctaagt-3' and 5'-
783 aacaggtctcatgttaactagagaatgtacggcttgttt-3' and cloned via Eco31I-
784 restriction sites into GreenGate entry module vector pGGA000
785 (Lampropoulos et al. 2013). Genomic fragment of *LOTR1* coding sequence
786 was amplified with 5'-
787 aacaggtctcaggctcgatgTCAGCTATTCATCTTAAAAACCAAACTTCA and 5'-
788 aacaggtctcaCTGAAGGACACCTTGGGTTCCG-3' and cloned into pGGC000.
789 mScarlet-I was amplified from pmScarlet-I_C1 (Bindels et al. 2016)

790 obtained from Addgene and secretion peptide was added by tandem PCR
791 amplification with 5'-
792 gctctttccctctatctcctgcccaatccagccactagtATGGTGAGCAAGGGCGAG-3' (FW1)
793 and 5'-
794 aacaGGTCTCaAACAatgaaagccttcacactcgctctcttcttagctctttccctctatctcctg-3'
795 (FW2) and 5'-aacaGGTCTCaAGCCCTTGTACAGCTCGTCCATGC-3' (RV) and
796 cloned via Eco31I sites into pGGB000. Final destination clones were
797 obtained by subsequent GoldenGate reaction with pGreenII based
798 pGGZ003 and transformed into *Arabidopsis* using floral dip.

799 *Confocal imaging*
800 Imaging was performed on Leica SP8 or Zeiss LSM880 microscopes,
801 excitation and emission as follows (excitation, detection): Calcofluor White
802 (405 nm, 425 – 475 nm), GFP (488nm, 500 – 550 nm),
803 mCherry/tdTomato/mScarlet-I (563 nm, 580 – 650 nm), PI (563 nm, 580 –
804 650 nm), basic Fuchsin (563 nm, 580 – 650 nm).

805 *PI assay*
806 PI was performed as described in Lee et al. 2013 with following changes:
807 Seedlings were incubated in 10 µg/ml PI dissolved in water for 5 min and
808 imaged immediately afterwards. Number of endodermal cells determined
809 after onset of elongation (defined as first endodermal cell with length to
810 width ratio of at least 2, i.e. at least twice as long than wide).

811 *Transmission electron microscopy (TEM)*

812 5-day-old Arabidopsis seedlings were fixed in glutaraldehyde solution
813 (EMS, Hatfield, PA) 2.5% in 100 mM phosphate buffer (pH 7.4) for 1 hour at
814 room temperature. Then, they were post-fixed in osmium tetroxide 1%
815 (EMS) with 1.5% of potassium ferrocyanide (Sigma, St. Louis, MO) in
816 phosphate buffer for 1 hour at room temperature. Following that, the
817 plants were rinsed twice in distilled water and dehydrated in ethanol
818 solution (Sigma) at gradient concentrations (30% 40 min; 50% 40 min; 70%
819 40 min; two times (100% 1 hour). This was followed by infiltration in Spurr
820 resin (EMS) at gradient concentrations (Spurr 33% in ethanol, 4 hours;

821 Spurr 66% in ethanol, 4 hours; Spurr two times (100% 8 hours) and finally
822 polymerized for 48 hours at 60℃ in an oven. Ultrathin sections 50 nm thick
823 were cut transversally at 2mm ± 0.2 mm from the root tip, on a Leica
824 Ultracut (Leica Mikrosysteme GmbH, Vienna, Austria) and two consecutive
825 sections were picked up on a nickel slot grid 2X1 mm (EMS) coated with a
826 polystyrene film (Sigma).

827 *Lignin staining with permanganate potassium ($KMnO_4$) using TEM*

828 Visualization of lignin deposition around Casparian strip was done using
829 permanganate potassium ($KMnO_4$) staining (Hepler, Fosket, and Newcomb
830 1970). The first section was imaged without any post-staining. Then the
831 sections were post-stained using 1% of $KMnO_4$ in H_2O (Sigma, St Louis, MO,
832 US) for 45min and rinsed several times with H_2O. Then the second section
833 of the grid was imaged. Micrographs were taken with a transmission
834 electron microscope FEI CM100 (FEI, Eindhoven, The Netherlands) at an
835 acceleration voltage of 80kV and 11000X magnifications (pixel size of
836 1.851nm), with a TVIPS TemCamF416 digital camera (TVIPS GmbH,
837 Gauting, Germany) using the software EM-MENU 4.0 (TVIPS GmbH,
838 Gauting, Germany). Panoramic were aligned with the software IMOD
839 (Kremer, Mastronarde, and McIntosh 1996).

840 *Cell ablation*

841 Endodermal cells were ablated using a MaiTai-SpectraPhysics laser at 800
842 nm integrated into a Zeiss LSM880 microscope. A ROI outlining the cells to
843 ablate was used and cells were ablated with 2 % power and 0.8 µs pixel
844 dwell time. Cell destruction was confirmed using transmitted light and PI
845 staining.

846 *Western blot*

847 Roots of 5-day old seedlings grown on ½ MS medium were cut and
848 weighted before shock-freezing in liquid nitrogen. Samples were then
849 homogenized using TissueLyser II (Qiagen). Proteins were then denatured
850 by addition of 3x (v/w) 1x NuPAGE LDS sample buffer + 50 mM DTT
851 (Invitrogen, NP0007) and heating for 5 min at 70 °C. Cell debris was

852 removed by centrifugation at 1’000 *g* for 5 min before separation of
853 proteins on pre-cast 12 % Bis-Tris SDS-PAGE gels (iD PAGE, Eurogentec).
854 After electrophoresis, proteins were transferred onto PVDF membrane
855 using Pierce FastBlotter G2 semi-dry blotting. Membranes were then
856 blocked (5 % skim milk in TBS) for 1 h before incubation with anti-RFP
857 antibody (1:1000, Chromotek 6G6) overnight at 4 °C. After washing the
858 membrane three times with 1x TBS + 0.1 % Tween (TBS-T), blot incubated
859 for 2 h at root temperature with anti-mouse-HRP antibody (1:5000).
860 Finally, after washing blot three times with TBS-T, HRP activity was
861 detected using SuperSignal West Femto Kit (Thermo Scientific) and GE
862 ImageQuant LAS 500.

863 *Phylogenetic analysis*

864 Homologs of LOTR1 were identified by searching the *Arabidopsis thaliana*
865 proteome for proteins containing both Neprosin-AP (PF14365) and
866 Neprosin domains (PF03080). Sequence similarity was compared using
867 MUSCLE (EMBL-EBI, Madeira et al. 2019). Phyolgenetic analysis was done
868 using the NGPhylogeny.fr online-tool with PhylML+SMS settings. Final tree
869 was assembled and annotated with iTOL online tool (Letunic and Bork
870 2019). Conserved residues were identified using pre-aligned sequences and
871 the online-weblogo tool from the University of Berkely
872 (https://weblogo.berkeley.edu/logo.cgi) (Crooks et al. 2004).

873 *Statistical analysis*

874 Statistical analysis was done in R software (R Core Team, 2013)
875 (https://www.r-project.org/). For multiple group comparisons, one-way
876 ANOVA was performed, and significantly different groups identified with
877 Tukey-Kramer post-hoc test.

878

879 **Fig. S1: Establishment of ectopic domain formations in *lotr1*.**

880 A Localization of ectopic deposition of CASP1-GFP (green). Section view of
881 z-stack through roots 5-10 cells after onset of protoxylem differentiation,
882 cell wall stained with Calcofluor White (white) and crops shown on top
883 outlined in overview pictures below (dashed yellow line); scale bar = 50
884 um, c = cortex, e = endodermis, p = pericycle.

885 B Quantification of ectopic CASP1-GFP patches. Number and position of
886 ectopic patches were determined per cell and depicted as ratio of patches
887 facing pericycle cells vs total patch number, maximum of 3 cells counted
888 per seedling, n_{total} = 11.

889 C Deposition of CASP1-GFP in *lotr1*. CASP1-GFP fluorescence depicted
890 throughout CSD formation in *lotr1*; scale bars = 5 um. Kymograph image at
891 bottom illustrates fluorescence over time in line indicated above, individual
892 patch formation visible as independent pyramid-like structures (yellow
893 arrows).

894 D TEM section of wildtype at 2 mm. Closeup indicated by dashed black line
895 in overview image, en = endodermis, pe = pericycle, scale bars = 2 µm.

896 E Consecutive TEM sections at 2 mm from root tip, with and without
897 $KMnO_4$ staining. Dark deposits indicate electron-dense MnO_2 precipitation
898 caused by reaction with lignin; en = endodermis, pe = pericycle, black
899 arrows indicate CS-like cell wall with attached plasma membranes, white
900 arrows highlight plasmolyzed membranes detached from the cell wall,
901 scale bar = 1 µm.

902

903 **Fig. S2: CASP1-GFP membrane coordination.**
904 Double membrane phenotype in CS mutants, scale bars = 5 um. R^2 value
905 depicts Spearman rho correlation coefficients of fluorescence of 5 pixel
906 wide lines following each membrane.

907

908 **Fig. S3: Cell ablation impacts CS establishment.**
909 A CASP1 promoter activity highlighted by nls-GFP (green) after ablation of
910 all neighboring cells prior to onset of expression, PI (red) outlines cells and
911 confirmed cell destruction. Scale bar = 50 um.

912 B Endodermal differentiation was induced via 0.5 µM β-estradiol and
913 CASP1-GFP expression (white) followed over the next 12 h. Red arrows
914 indicate unstable CASP deposits in the membrane, scale bar = 50 um.

915 C CSD formation in wildtype and *lotr1*. Single endodermal cells ablated 3-4
916 cells prior to onset of CASP expression, * depicts ablated cell, scale bar = 50
917 um.

918

919 **Fig. S4: Investigation of putative post-translational processing in LOTR1.**

920 A Lignin accumulation (magenta) in wildtype and *sgn3* with CSDs labelled
921 by CASP1-GFP (green).

922 B Schematic view of LOTR1 with position of identified loss-of-function
923 alleles indicated.

924 C Processing of LOTR1. Root protein extracts separated via SDS-PAGE and
925 LOTR1-fragments detected by anti-RFP antibody (Chromotek 6G6). Note
926 that C-terminal fusion construct LOTR1::LOTR1-mCherry does not
927 complement the *lotr1* phenotype, but shows processing/degradation
928 fragments. Both weak (#1) and strong (#2) C-terminal complementation
929 lines lack processing/degradation fragments.

930 D Complementation analysis of the *lotr1* CASP1-GFP phenotype using
931 truncated versions consisting of only LOTR1's Neprosin domain (Neprosin),
932 the putative autoinhibitory Neprosin-AP domain (Neprosin-AP), or full-
933 length LOTR1 with conserved cysteines C255 and C260 mutated
934 ($LOTR1^{C255A,C260A}$), scale bars = 50 µm.

935

936 **Fig. S5: Neprosin domain analysis in the HOLO family.**
937 A Conservation of Neprosin domain throughout the HOLO-family, including
938 LOTR1. Putative catalytic triade amino acids aligning with *E.coli* mepS
939 marked with red arrows.

940 B Sequence alignment of *E.coli* mepS, Neprosin, LOTR1 and its closest
941 homologs At1g23340 (HOLO2), At1g70550 (HOLO3), and At1g10750
942 (HOLO4)

943

944

945 **References**

946 Alassimone, J, S Fujita, V G Doblas, M van Dop, M Barberon, L Kalmbach, J E
947 Vermeer, et al. 2016. "Polarly Localized Kinase SGN1 Is Required for
948 Casparian Strip Integrity and Positioning." *Nat Plants* 2: 16113.
949 https://doi.org/10.1038/nplants.2016.113.

950 Alassimone, Julien, Sadaf Naseer, and Niko Geldner. 2010. "A
951 Developmental Framework for Endodermal Differentiation and
952 Polarity." *Proc Natl Acad Sci U S A* 107 (11): 5214–19.
953 https://doi.org/10.1073/pnas.0910772107.

954 Bao, Zhulatai, Juan Bai, Hongchang Cui, and Chunmei Gong. 2019. "A
955 Missing Link in Radial Ion Transport: Ion Transporters in the
956 Endodermis." *Frontiers in Plant Science* 10 (June): 1–8.
957 https://doi.org/10.3389/fpls.2019.00713.

958 Barbosa, Inês Catarina Ramos, Nelson Rojas-Murcia, and Niko Geldner.
959 2019. "The Casparian Strip—One Ring to Bring Cell Biology to
960 Lignification?" *Current Opinion in Biotechnology* 56: 121–29.
961 https://doi.org/10.1016/j.copbio.2018.10.004.

962 Bindels, Daphne S., Lindsay Haarbosch, Laura Van Weeren, Marten Postma,
963 Katrin E. Wiese, Marieke Mastop, Sylvain Aumonier, et al. 2016.
964 "MScarlet: A Bright Monomeric Red Fluorescent Protein for Cellular
965 Imaging." *Nature Methods*. https://doi.org/10.1038/nmeth.4074.

966 Crooks, Gavin E, Gary Hon, John Marc Chandonia, and Steven E. Brenner.
967 2004. "WebLogo: A Sequence Logo Generator." *Genome Research* 14
968 (6): 1188–90. https://doi.org/10.1101/gr.849004.

969 Denyer, Tom, Xiaoli Ma, Simon Klesen, Emanuele Scacchi, Kay Nieselt, and
970 Marja C.P. Timmermans. 2019. "Spatiotemporal Developmental
971 Trajectories in the Arabidopsis Root Revealed Using High-Throughput
972 Single-Cell RNA Sequencing." *Developmental Cell* 48 (6): 840-852.e5.
973 https://doi.org/10.1016/j.devcel.2019.02.022.

974 Doblas, Verónica G, Elwira Smakowska-Luzan, Satoshi Fujita, Julien

975 Alassimone, Marie Barberon, Mathias Madalinski, Youssef Belkhadir,
976 and Niko Geldner. 2017. “Root Diffusion Barrier Control by a
977 Vasculature-Derived Peptide Binding to the SGN3 Receptor.” *Science*
978 355 (6322): 280–84. https://doi.org/10.1126/science.aaj1562.

979 Enstone, Daryl E., Carol A. Peterson, and Fengshan Ma. 2002. “Root
980 Endodermis and Exodermis: Structure, Function, and Responses to the
981 Environment.” *Journal of Plant Growth Regulation*. Springer.
982 https://doi.org/10.1007/s00344-003-0002-2.

983 Fujita, Satoshi, Damien De Bellis, Kai H Edel, Philipp Köster, Tonni Grube
984 Andersen, Emanuel Schmid-Siegert, Valérie Dénervaud Tendon, et al.
985 2020. “SCHENGEN Receptor Module Drives Localized ROS Production
986 and Lignification in Plant Roots.” *The EMBO Journal*, e103894.
987 https://doi.org/10.15252/embj.2019103894.

988 Geldner, Niko. 2013. “The Endodermis.” *Annual Review of Plant Biology* 64
989 (1): 531–58. https://doi.org/10.1146/annurev-arplant-050312-
990 120050.

991 Hepler, Peter K., Donald E. Fosket, and Eldon H. Newcomb. 1970.
992 “LIGNIFICATION DURING SECONDARY WALL FORMATION IN COLEUS:
993 AN ELECTRON MICROSCOPIC STUDY.” *American Journal of Botany* 57
994 (1): 85–96. https://doi.org/10.1002/j.1537-2197.1970.tb09793.x.

995 Hosmani, P S, T Kamiya, J Danku, S Naseer, N Geldner, M L Guerinot, and D
996 E Salt. 2013. “Dirigent Domain-Containing Protein Is Part of the
997 Machinery Required for Formation of the Lignin-Based Casparian Strip
998 in the Root.” *Proc Natl Acad Sci U S A* 110 (35): 14498–503.
999 https://doi.org/10.1073/pnas.1308412110.

1000 Itoh, Masahiko, and Mina J. Bissell. 2003. “The Organization of Tight
1001 Junctions in Epithelia: Implications for Mammary Gland Biology and
1002 Breast Tumorigenesis.” *Journal of Mammary Gland Biology and*
1003 *Neoplasia* 8 (4): 449–62.
1004 https://doi.org/10.1023/B:JOMG.0000017431.45314.07.

1005 Kalmbach, L, K Hematy, D De Bellis, M Barberon, S Fujita, R Ursache, J
1006 Daraspe, and N Geldner. 2017. “Transient Cell-Specific EXO70A1
1007 Activity in the CASP Domain and Casparian Strip Localization.” *Nat*
1008 *Plants* 3: 17058. https://doi.org/10.1038/nplants.2017.58.

1009 Kamiya, Takehiro, Monica Borghi, Peng Wang, John M. C. Danku, Lothar
1010 Kalmbach, Prashant S. Hosmani, Sadaf Naseer, Toru Fujiwara, Niko
1011 Geldner, and David E. Salt. 2015. “The MYB36 Transcription Factor
1012 Orchestrates Casparian Strip Formation.” *Proc Natl Acad Sci U S A* 112
1013 (33): 10533–38. https://doi.org/10.1073/pnas.1507691112.

1014 Kremer, James R, David N Mastronarde, and J.Richard McIntosh. 1996.
1015 “Computer Visualization of Three-Dimensional Image Data Using
1016 IMOD.” *Journal of Structural Biology* 116 (1): 71–76.
1017 https://doi.org/10.1006/jsbi.1996.0013.

1018 Lampropoulos, A, Z Sutikovic, C Wenzl, I Maegele, J U Lohmann, and J
1019 Forner. 2013. “GreenGate---a Novel, Versatile, and Efficient Cloning
1020 System for Plant Transgenesis.” *PLoS One* 8 (12): e83043.
1021 https://doi.org/10.1371/journal.pone.0083043.

1022 Lee, Y, M C Rubio, J Alassimone, and N Geldner. 2013. “A Mechanism for
1023 Localized Lignin Deposition in the Endodermis.” *Cell* 153 (2): 402–12.
1024 https://doi.org/10.1016/j.cell.2013.02.045.

1025 Letunic, Ivica, and Peer Bork. 2019. “Interactive Tree of Life (ITOL) v4:
1026 Recent Updates and New Developments.” *Nucleic Acids Research*.
1027 https://doi.org/10.1093/nar/gkz239.

1028 Li, B, T Kamiya, L Kalmbach, M Yamagami, K Yamaguchi, S Shigenobu, S
1029 Sawa, et al. 2017. “Role of LOTR1 in Nutrient Transport through
1030 Organization of Spatial Distribution of Root Endodermal Barriers.” *Curr*
1031 *Biol* 27 (5): 758–65. https://doi.org/10.1016/j.cub.2017.01.030.

1032 Liberman, L M, E E Sparks, M A Moreno-Risueno, J J Petricka, and P N
1033 Benfey. 2015. “MYB36 Regulates the Transition from Proliferation to
1034 Differentiation in the Arabidopsis Root.” *Proc Natl Acad Sci U S A* 112

1035 (39): 12099–104. https://doi.org/10.1073/pnas.1515576112.

1036 Ma, Jian Feng, Naoki Yamaji, Namiki Mitani, Kazunori Tamai, Saeko Konishi,
1037 Toru Fujiwara, Maki Katsuhara, and Masahiro Yano. 2007. "An Efflux
1038 Transporter of Silicon in Rice." *Nature*.
1039 https://doi.org/10.1038/nature05964.

1040 Madeira, Fábio, Young Mi Park, Joon Lee, Nicola Buso, Tamer Gur, Nandana
1041 Madhusoodanan, Prasad Basutkar, et al. 2019. "The EMBL-EBI Search
1042 and Sequence Analysis Tools APIs in 2019." *Nucleic Acids Research*.
1043 https://doi.org/10.1093/nar/gkz268.

1044 Marhavý, Peter, and Eva Benková. 2015. "Real-Time Analysis of Lateral
1045 Root Organogenesis in Arabidopsis." *BIO-PROTOCOL* 5 (8).
1046 https://doi.org/10.21769/BioProtoc.1446.

1047 Marhavý, Peter, Juan Carlos Montesinos, Anas Abuzeineh, Daniel Van
1048 Damme, Joop E.M. Vermeer, Jerôme Duclercq, Hana Rakusová, et al.
1049 2016. "Targeted Cell Elimination Reveals an Auxin-Guided Biphasic
1050 Mode of Lateral Root Initiation." *Genes and Development* 30 (4): 471–
1051 83. https://doi.org/10.1101/gad.276964.115.

1052 Nakayama, Takuya, Hidefumi Shinohara, Mina Tanaka, Koki Baba, Mari
1053 Ogawa-Ohnishi, and Yoshikatsu Matsubayashi. 2017. "A Peptide
1054 Hormone Required for Casparian Strip Diffusion Barrier Formation in
1055 Arabidopsis Roots." *Science* 355 (6322): 284–86.
1056 https://doi.org/10.1126/science.aai9057.

1057 Naseer, S, Y Lee, C Lapierre, R Franke, C Nawrath, and N Geldner. 2012.
1058 "Casparian Strip Diffusion Barrier in Arabidopsis Is Made of a Lignin
1059 Polymer without Suberin." *Proc Natl Acad Sci U S A* 109 (25): 10101–6.
1060 https://doi.org/10.1073/pnas.1205726109.

1061 Pfister, A, M Barberon, J Alassimone, L Kalmbach, Y Lee, J E Vermeer, M
1062 Yamazaki, et al. 2014. "A Receptor-like Kinase Mutant with Absent
1063 Endodermal Diffusion Barrier Displays Selective Nutrient Homeostasis
1064 Defects." *Elife* 3: e03115. https://doi.org/10.7554/eLife.03115.

1065 Rajasekaran, Ayyappan K., Minoru Hojo, Tellervo Huima, and Enrique
1066 Rodriguez-Boulan. 1996. “Catenins and Zonula Occludens-1 Form a
1067 Complex during Early Stages in the Assembly of Tight Junctions.”
1068 *Journal of Cell Biology* 132 (3): 451–63.
1069 https://doi.org/10.1083/jcb.132.3.451.

1070 Rey, M, M Yang, L Lee, Y Zhang, J G Sheff, C W Sensen, H Mrazek, et al.
1071 2016. “Addressing Proteolytic Efficiency in Enzymatic Degradation
1072 Therapy for Celiac Disease.” *Sci Rep* 6: 30980.
1073 https://doi.org/10.1038/srep30980.

1074 Roppolo, Daniele, Bert De Rybel, Valérie Dénervaud Tendon, Alexandre
1075 Pfister, Julien Alassimone, Joop E. M. Vermeer, Misako Yamazaki,
1076 York-Dieter Stierhof, Tom Beeckman, and Niko Geldner. 2011. “A
1077 Novel Protein Family Mediates Casparian Strip Formation in the
1078 Endodermis.” *Nature* 473 (7347): 380–83.
1079 https://doi.org/10.1038/nature10070.

1080 Ryu, K H, L Huang, H M Kang, and J Schiefelbein. 2019. “Single-Cell RNA
1081 Sequencing Resolves Molecular Relationships Among Individual Plant
1082 Cells.” *Plant Physiol* 179 (4): 1444–56.
1083 https://doi.org/10.1104/pp.18.01482.

1084 Schrader, C U, L Lee, M Rey, V Sarpe, P Man, S Sharma, V Zabrouskov, B
1085 Larsen, and D C Schriemer. 2017. “Neprosin, a Selective Prolyl
1086 Endoprotease for Bottom-up Proteomics and Histone Mapping.” *Mol*
1087 *Cell Proteomics* 16 (6): 1162–71.
1088 https://doi.org/10.1074/mcp.M116.066803.

1089 Siligato, R, X Wang, S R Yadav, S Lehesranta, G Ma, R Ursache, I Sevilem, et
1090 al. 2016. “MultiSite Gateway-Compatible Cell Type-Specific Gene-
1091 Inducible System for Plants.” *Plant Physiol* 170 (2): 627–41.
1092 https://doi.org/10.1104/pp.15.01246.

1093 Stein, Barry D., Karen L. Klomparens, and Raymond Hammerschmidt. 1992.
1094 “Comparison of Bromine and Permanganate as Ultrastructural Stains
1095 for Lignin in Plants Infected by the FungusColletotrichum

1096 Lagenarium." *Microscopy Research and Technique* 23 (3): 201–6.
1097 https://doi.org/10.1002/jemt.1070230302.

1098 Takano, Junpei, Mayuki Tanaka, Atsushi Toyoda, Kyoko Miwa, Koji Kasai,
1099 Kentaro Fuji, Hitoshi Onouchi, Satoshi Naito, and Toru Fujiwara. 2010.
1100 "Polar Localization and Degradation of Arabidopsis Boron
1101 Transporters through Distinct Trafficking Pathways." *Proceedings of*
1102 *the National Academy of Sciences of the United States of America*.
1103 https://doi.org/10.1073/pnas.0910744107.

1104 Ursache, R, T G Andersen, P Marhavy, and N Geldner. 2018. "A Protocol for
1105 Combining Fluorescent Proteins with Histological Stains for Diverse
1106 Cell Wall Components." *Plant J* 93 (2): 399–412.
1107 https://doi.org/10.1111/tpj.13784.

1108 Yamashita, Daichi, Satoshi Kimura, Masahisa Wada, and Keiji Takabe. 2016.
1109 "Improved Mäule Color Reaction Provides More Detailed Information
1110 on Syringyl Lignin Distribution in Hardwood." *Journal of Wood Science*
1111 62 (2): 131–37. https://doi.org/10.1007/s10086-016-1536-9.

1112 Zuo, Jianru, Qi-Wen W. Niu, and Nam-Hai H. Chua. 2000. "An Estrogen
1113 Receptor-Based Transactivator XVE Mediates Highly Inducible Gene
1114 Expression in Transgenic Plants." *The Plant Journal* 24 (2): 265–73.
1115 https://doi.org/10.1046/j.1365-313x.2000.00868.x.

1116

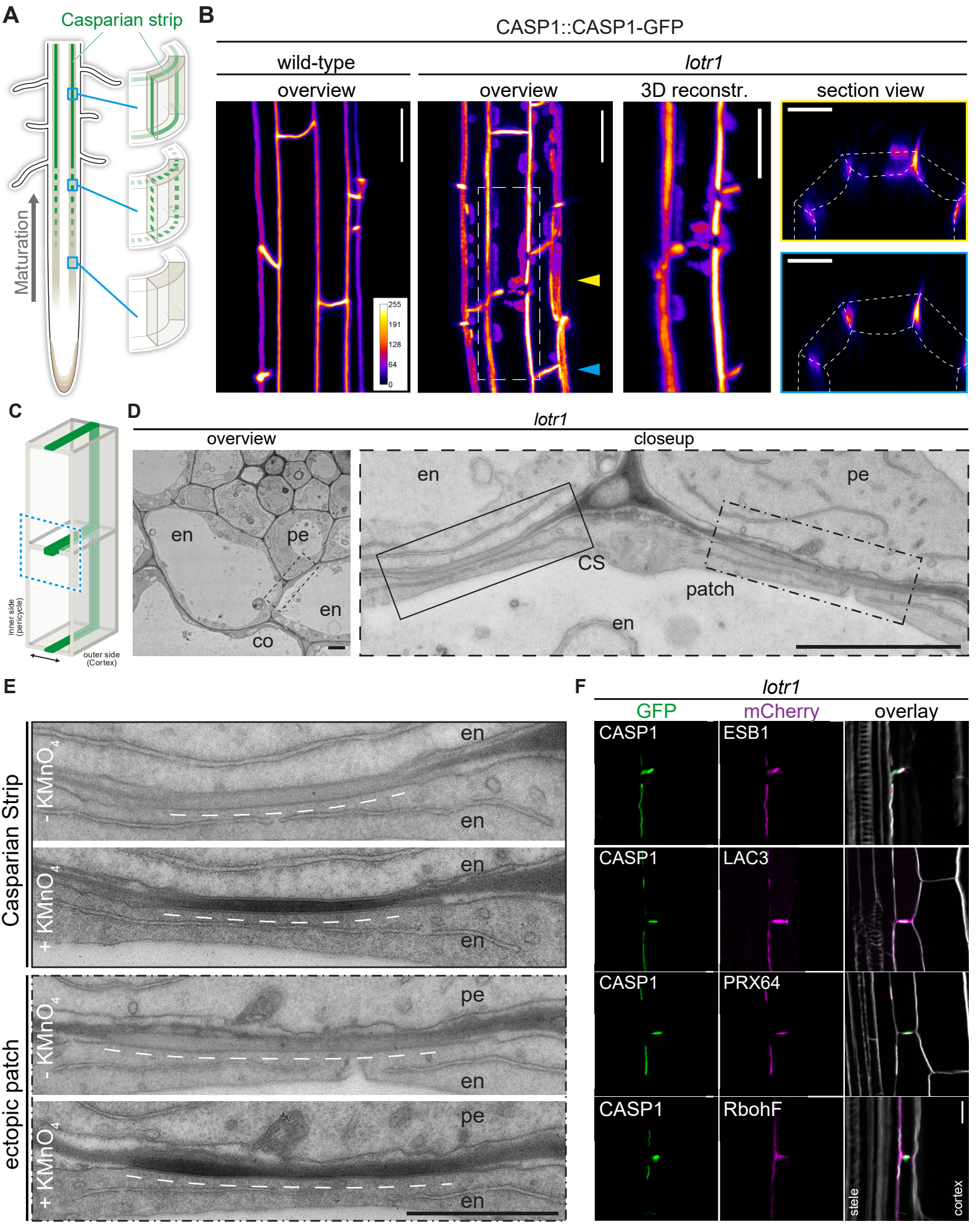
A
Casparian strip
Maturation
B
CASP1::CASP1-GFP
wild-type
lotr1
overview
overview
3D reconstr.
section view
255
191
128
64
0
C
inner side (pericycle)
outer side (Cortex)
D
lotr1
overview
closeup
en
pe
en
co
en
pe
CS
patch
en
E
lotr1
Casparian Strip
ectopic patch
- KMnO4
+ KMnO4
- KMnO4
+ KMnO4
en
en
en
en
pe
en
pe
en
F
lotr1
GFP
mCherry
overlay
CASP1
ESB1
CASP1
LAC3
CASP1
PRX64
CASP1
RbohF
stele
cortex

Fig. 1

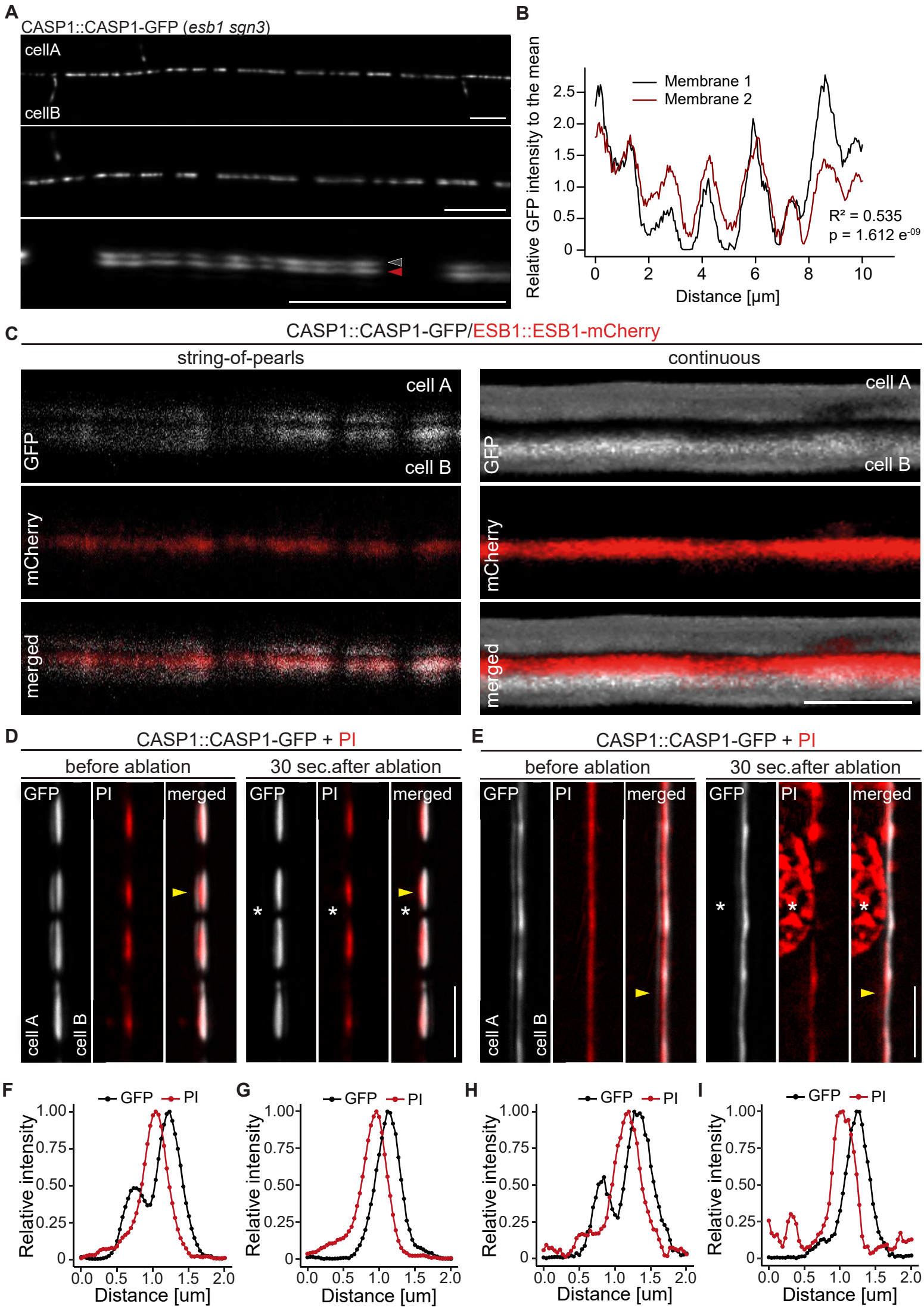
A
CASP1::CASP1-GFP (esb1 sqn3)
cellA
cellB
B
Membrane 1
Membrane 2
Relative GFP intensity to the mean
R² = 0.535
p = 1.612 e-09
Distance [µm]
C
CASP1::CASP1-GFP/ESB1::ESB1-mCherry
string-of-pearls
continuous
cell A
cell B
GFP
mCherry
merged
D
CASP1::CASP1-GFP + PI
before ablation
30 sec.after ablation
GFP
PI
merged
cell A
cell B
E
CASP1::CASP1-GFP + PI
before ablation
30 sec.after ablation
F
G
H
I
Relative intensity
Distance [um]

Fig. 2

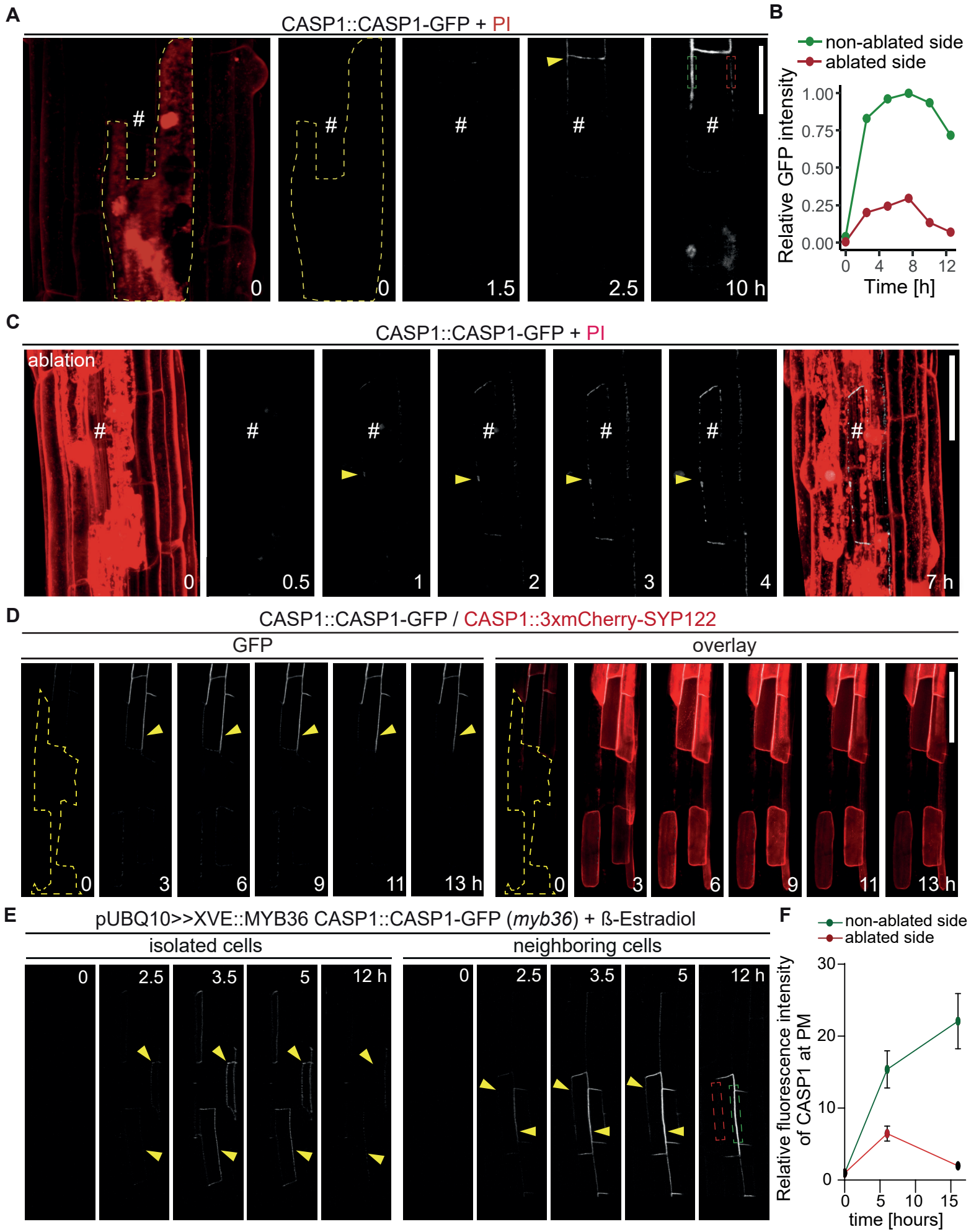
A
CASP1::CASP1-GFP + PI
#
0
0
1.5
2.5
10 h
B
non-ablated side
ablated side
Relative GFP intensity
1.00
0.75
0.50
0.25
0.00
0
4
8
12
Time [h]
C
CASP1::CASP1-GFP + PI
ablation
0
0.5
1
2
3
4
7 h
D
CASP1::CASP1-GFP / CASP1::3xmCherry-SYP122
GFP
overlay
0
3
6
9
11
13 h
E
pUBQ10>>XVE::MYB36 CASP1::CASP1-GFP (myb36) + ß-Estradiol
isolated cells
neighboring cells
0
2.5
3.5
5
12 h
F
non-ablated side
ablated side
Relative fluorescence intensity of CASP1 at PM
30
20
10
0
0
5
10
15
time [hours]

Fig. 3

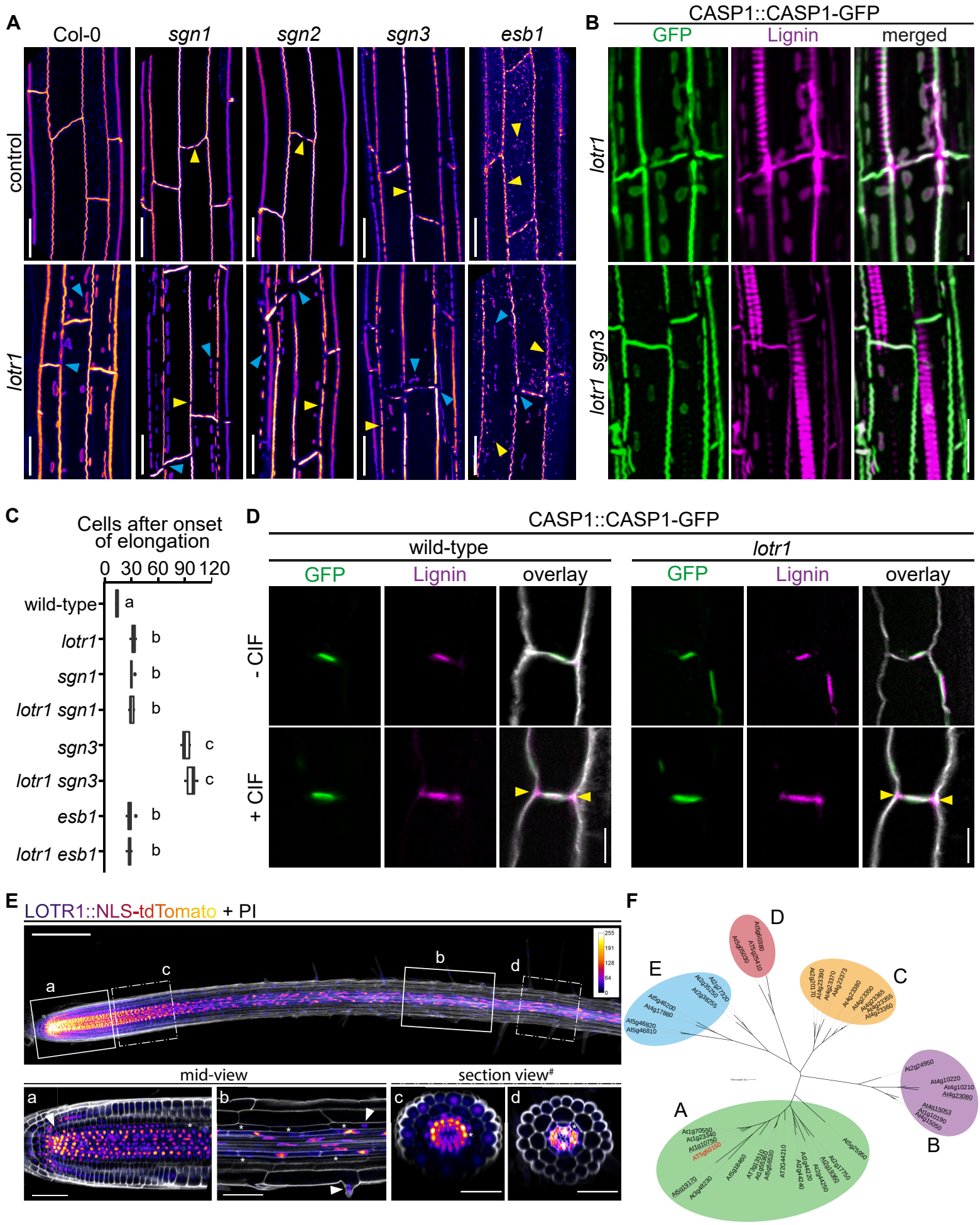
A
Col-0
sgn1
sgn2
sgn3
esb1
control
lotr1
B
CASP1::CASP1-GFP
GFP
Lignin
merged
lotr1
lotr1 sgn3
C
Cells after onset of elongation
0 30 60 90 120
wild-type
lotr1
sgn1
lotr1 sgn1
sgn3
lotr1 sgn3
esb1
lotr1 esb1
a
b
b
b
c
c
b
b
D
CASP1::CASP1-GFP
wild-type
lotr1
GFP
Lignin
overlay
- CIF
+ CIF
E
LOTR1::NLS-tdTomato + PI
a
c
b
d
mid-view
section view#
F
A
B
C
D
E

Fig. 4

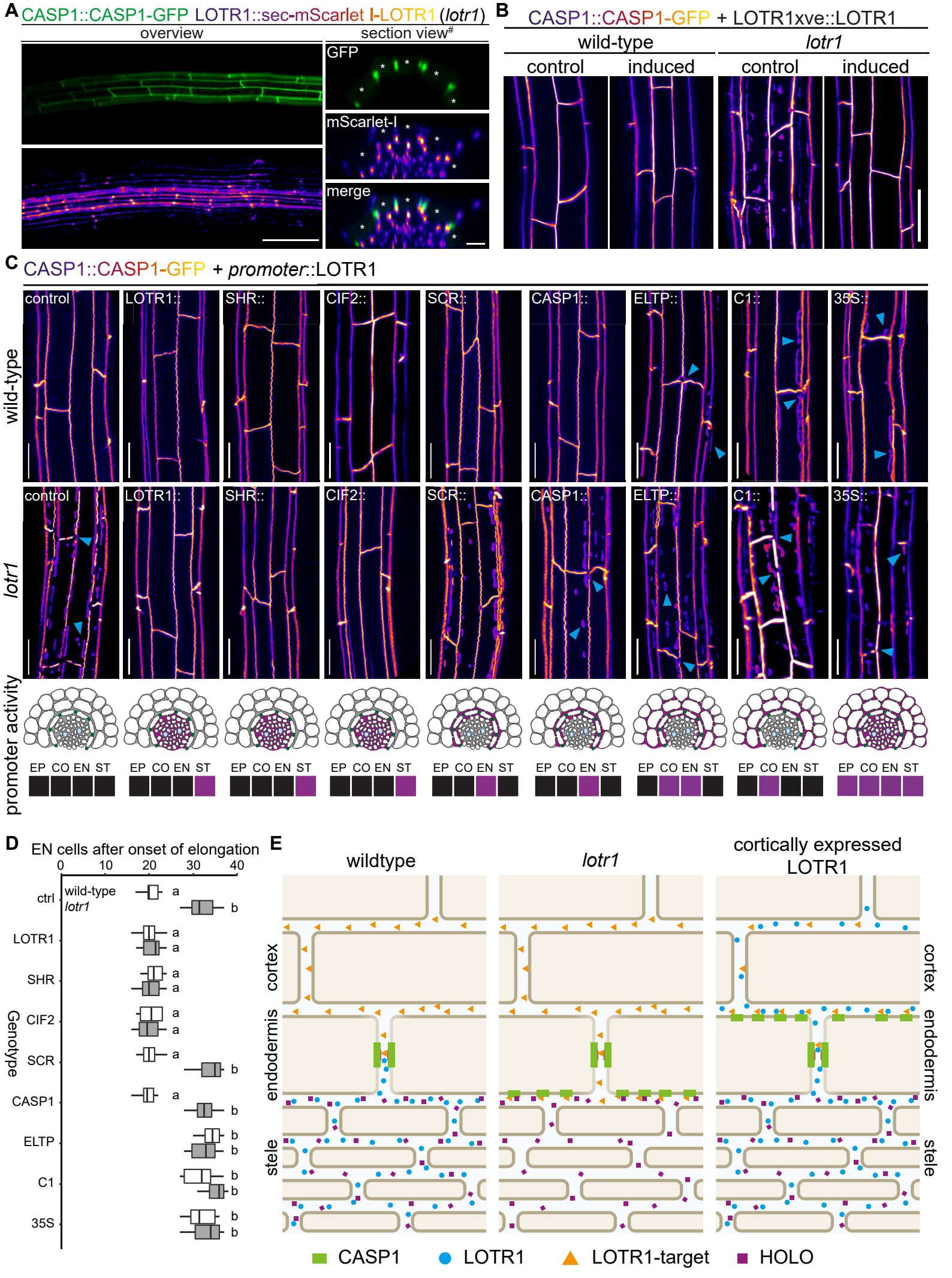
A
CASP1::CASP1-GFP LOTR1::sec-mScarlet I-LOTR1 (lotr1)
overview
section view#
GFP
mScarlet-I
merge
B
CASP1::CASP1-GFP + LOTR1xve::LOTR1
wild-type
lotr1
control
induced
control
induced
C
CASP1::CASP1-GFP + promoter::LOTR1
wild-type
lotr1
promoter activity
control
LOTR1::
SHR::
CIF2::
SCR::
CASP1::
ELTP::
C1::
35S::
EP CO EN ST
D
EN cells after onset of elongation
0
10
20
30
40
Genotype
ctrl
LOTR1
SHR
CIF2
SCR
CASP1
ELTP
C1
35S
wild-type
lotr1
a
b
E
wildtype
lotr1
cortically expressed LOTR1
cortex
endodermis
stele
CASP1
LOTR1
LOTR1-target
HOLO

Fig. 5